A master-slave coupling scheme for synchronization and parameter estimation in the generalized Kuramoto-Sivashinsky equation

Joaquín Miguez

Department of Signal Theory & Communications,

Universidad Carlos III de Madrid (Spain) and

Instituto de Investigación Sanitaria Gregorio Marañón (Spain)

Harold Molina-Bulla

Department of Signal Theory & Communications,

Universidad Carlos III de Madrid (Spain)

Inés P. Mariño

Department of Biology & Geology, Physics and Inorganic Chemistry,

Universidad Rey Juan Carlos (Spain) and

Department of Women's Cancer, University College London (UK)

(*joaquin.miguez@uc3m.es, hmolina@tsc.uc3m.es, ines.perez@urjc.es)

(Dated: August 9, 2024)

Abstract

The problem of estimating the constant parameters of the Kuramoto-Sivashinsky (KS) equation from observed data has received attention from researchers in physics, applied mathematics and statistics. This is motivated by the various physical applications of the equation and, also, because it often serves as a test model for the study of space-time pattern formation. Remarkably, most existing inference techniques rely on statistical tools, which are computationally very costly yet do not exploit the dynamical features of the system. In this paper we introduce a simple, online parameter estimation method that relies on the synchronization properties of the KS equation. In particular, we describe a master-slave setup where the slave model is driven by observations from the master system. The slave dynamics are data-driven and designed to continuously adapt the model parameters until identical synchronization with the master system is achieved. We provide a simple analysis that supports the proposed approach and also present and discuss the results of an extensive set of computer simulations. Our numerical study shows that the proposed method is computationally fast and also robust to initialization errors, observational noise and variations in the spatial resolution of the numerical scheme used to integrate the KS equation.

I. INTRODUCTION

A. The Kuramoto-Sivashinsky equation

The Kuramoto-Sivashinsky (KS) equation is a partial differential equation (PDE) that describes the spatio-temporal evolution of certain nonlinear systems. It was independently developed by Y. Kuramoto [1, 2], to model waves in Belousov–Zhabotinsky reactions, and A. Sivashinsky [3, 4] to study instabilities in laminar flame fronts. Other significant applications include the modeling of liquid films [5], long waves in viscous fluids [6], drift waves in plasmas [7] or ion-sputtered surfaces [8].

The generalized KS equation in 1-dimensional space can be written as [9]

$$u_t + uu_x + \alpha u_{xx} + \beta u_{xxx} + \gamma u_{xxxx} = 0, \tag{1}$$

where $t \in \mathbb{R}$ and $x \in \mathbb{R}$ are continuous time and space, respectively, $u(t,x)$ is a scalar field representing the physical magnitude of interest, $u_t = \frac{\partial u}{\partial t}$, $u_{xx} = \frac{\partial^2 u}{\partial x^2}$, $u_{xxx} = \frac{\partial^3 u}{\partial x^3}$, $u_{xxxx} = \frac{\partial^4 u}{\partial x^4}$, and the constants $\alpha, \beta, \gamma \in \mathbb{R}$ determine the dynamics of the signal $u(x,t)$. This equation has received considerable attention because it displays a rich space-time behavior, including chaotic dynamics,

depending on the choice of parameter values [10–15]

B. Parameter estimation for the KS model

The problem of estimating the values of the constant parameters (α, β, γ) from observations of the signal $u(t,x)$ is of interest because of the physical applications of the KS equation and also because this model has become a testbed to assess inference techniques that can then be applied to other spatially-extended systems.

Most parameter estimation methods designed for the KS model rely on statistical tools. Hurst *et al.* [16] describe a maximum likelihood (ML) inference scheme that runs an ensemble of Kalman-based estimators. Huttunen *et al.* [17] rely on a Fourier spectral decomposition of the KS equation with periodic boundary conditions. The Fourier series is truncated to K modes and an *ad hoc* noise term is added to the Fourier coefficients. Inference on the signal and the parameters is carried out by way of extended Kalman filtering and an importance sampling step. Lu *et al.* [18] start from a similar approach (a truncated Fourier-series representation) and then approximate the dynamics of the Fourier modes by way of an autoregressive time-series model. Martina-Perez *et al.* [19] also advocate a statistical scheme. They rely on the approximation of the PDE by way of a pre-selected set of basis functions and then tackle the Bayesian estimation of the basis dimension and the basis coefficients from the observed data.

Other methods include the use of deep learning schemes [20], a joint smoothing and parameter estimation method that aims at estimating both the solution $u(t,x)$ and the parameters (α, β, γ) using a quasi-Newton optimization algorithm [21] or a nonlinear least-squares fitting scheme that relies on the ability to simulate batches of data using a kinetic Monte Carlo procedure [22]. These schemes are offline (i.e., they require the iterative batch processing of the whole set of observations) and [20] requires an offline training stage before it can be applied.

All the methodologies described above share two limitations:

- they do not exploit the specific dynamics of the KS model and, as a consequence,
- they are computationally demanding –at least when compared with typical numerical integration schemes for the KS equation.

An alternative approach to the parameter estimation problem that has proved successful for chaotic dynamical models relies on the ability to synchronize two suitably coupled systems. In

a typical setup, one assumes that the observed data are generated by a *master* system with unknown parameters. The observations are used to drive a *slave* model that has the same form as the master system plus a coupling term that depends on the discrepancy between the two systems. The coupling is chosen in such a way that the slave model synchronizes with the master when the two systems are identical, including their parameters. Hence, the problem of parameter estimation reduces to finding the parameter values in the slave model that make the synchronization error vanish.

The general strategy described above, in different forms, has been advocated by several authors, e.g., in [21, 23–32]. However, it is hard to find applications of these methodologies to the KS equation. Most authors choose the Lorenz 63/96 or Rössler models to test their techniques [21, 23–28] (let us note that the KS equation is indeed considered as a case study in [21] but this is done only to show synchronization of a KS slave model with *known* parameters $\alpha = \gamma = 1$ and $\beta = 0$, while parameter estimation is tackled by other means). An outstanding exception is the recent work by Pachev *et al.* [30], who propose a synchronization-based procedure to estimate the parameters of a KS system online (i.e., concurrently with the numerical integration of the model). The main drawback of the method in [30] is that it requires the time derivatives of the observed signals, which are hard to estimate reliably in the presence of observational noise. In addition, their method also runs a Gram-Schmidt orthogonalization procedure and solves a system of linear equations at each time step of the numerical integration scheme –which results in a significant computational cost.

Master-slave synchronization of KS systems has been specifically shown and investigated, e.g., in [33, 34], and synchronization-based data assimilation schemes (aimed at the tracking and forecasting of the signal $u(t,x)$) have been proposed in [35–37]. In all these references, however, the parameters of the KS model are assumed known –there is no parameter estimation.

C. Contributions

The parameter estimation method introduced in this paper relies on a master-slave setup, similar to the general schemes of [30] and [26, 27]. Both the master and slave systems are KS models with periodic boundary conditions and they are approximated with truncated Fourier series: the master model is represented with M time-varying Fourier coefficients and we construct a slave model with K coefficients, $K \leq M$. We assume that the state $u(t,x)$ of the master system can be

observed over a spatial grid $x_0, \ldots, x_{J-1}$ and the collected data $u(t, x_j)$, $j = 0, \ldots, J-1$, are used to drive the slave system via a diffusive coupling term. We prove that this configuration yields local synchronization (according to the definition in [38]) when the parameters (α, β, γ) are identical in the master and slave models. We also show numerically that the scheme is robust, in the sense that synchronization is attained even when the initial conditions of the master and slave model differ significantly.

A key difference with the method in [30] lies in the parameter update rule. In the scheme introduced in this paper, the parameters of the slave model evolve continuously over time according to an ODE designed to have a stationary point where identical synchronization of the master and slave models is attained. In particular, there is no need for Gram-Schmidt orthogonalization steps and the computation of time derivatives of the observables is explicitly avoided. The slave parameters are integrated numerically with the same procedure used to integrate the Fourier coefficients of the master and slave models.

We present a detailed numerical assessment of the proposed synchronization-based parameter estimation scheme. In particular, we study

- the robustness of the method to initial errors in the slave model and the effect of the coupling strength;
- the robustness of the synchronization scheme and the parameter estimation method to observational noise in the data collected from the master system;
- the adaptation rate of the parameters, i.e., how quickly they converge to the master parameter values;
- the effect of underestimating the number of significant Fourier coefficients M in the master system, i.e., the performance of the proposed scheme when $K < M$;
- the relative accuracy and computational cost of the proposed scheme compared to the unscented Bucy-Kalman filter; and
- the performance of the parameter estimation method for different dynamical regimes (chaotic and periodic) of the master system.

D. Organization of the paper

The rest of this paper is organized as follows. A master-slave scheme that guarantees local identical synchronization is described in Section II. The parameter estimation methodology is introduced in Section III, which also includes an extensive set of computer simulation results. Finally, Section IV is devoted to a summary and a brief discussion of the methodology.

II. SYNCHRONIZATION OF GENERALIZED KURAMOTO-SIVASHINSKY MODELS

A. Master model

The methods described in this paper rely on a master-slave setup. The master system is described by Eq. (1) and we are interested on the evolution of the scalar field $u(t,x)$ during a time interval of length T, namely for $t \in [0,T]$. We assume a periodic boundary condition of the form $u(t,x) = u(t,x+X)$, for all $t \in [0,T]$ and some $X < \infty$, and denote the initial condition as $u_0(x) := u(0,x)$. The parameters of the master model (α, β, γ) are constant and assumed unknown.

The periodic-in-space field $u(t,x)$ can be equivalently represented by its time-varying Fourier series coefficients $\{a_k(t) : k \in \mathbb{Z}\}$ [39]. To be specific, if we let $\phi_k(x) := \exp\left\{i\frac{2\pi}{X}kx\right\}$ for $k \in \mathbb{Z}$ then we can write

$$u(x,t) = \sum_{k=-\infty}^{\infty} a_k(t)\phi_k(x), \tag{2}$$

for $t \in [0,T]$ and $x \in \mathbb{R}$. If we substitute (2) into (1), multiply by $\phi_k^*(x)$ and integrate over $x \in [0,X)$ on both sides of the equation, then we arrive at the infinite system of nonlinear ordinary differential equations (ODEs)

$$\dot{a}_k = a_k\left(\alpha\omega_0^2k^2 + i\beta\omega_0^3k^3 - \gamma\omega_0^4k^4\right) - \frac{1}{2}ik\omega_0\sum_{\ell=-\infty}^{\infty} a_\ell a_{k-\ell}, \tag{3}$$

for $k \in \mathbb{Z}$, where $\omega_0 = \frac{2\pi}{X}$. We restrict our attention to real fields, $u(t,x) \in \mathbb{R}$ for all x and $t \in [0,T]$, hence the Fourier coefficients are Hermitian, $a_k(t) = a_{-k}^*(t)$, and the one-sided sequence $\{a_k(t) : k = 0,1,2,\ldots\}$ determines the signal $u(t,x)$.

B. Slave model

Assume that the master model can be observed at a grid of spatial locations $x_0,\ldots,x_{J-1} \in [0,X)$ during the time interval $t \in [0,T]$, i.e., we collect measurements $u(t,x_j)$, $j = 0,\ldots,J-1$.

It is possible to use these observations to estimate the Fourier coefficients of the signal $u(t,x)$. Specifically, let us assume a truncation of Eq. (2) to the first K harmonics. Provided that $J \geq 2K+1$ and assuming that $u(t,x) \in \mathbb{R}$ (hence $a_k(t) = a_{-k}^*(t)$), it is possible to estimate the coefficients $a_0(t), \ldots, a_K(t)$ by solving the linear least-squares (LS) problem

$$\min_{\tilde{a}_k(t), k \geq 0} \sum_{j=0}^{J-1} \left| u(t,x_j) - \tilde{a}_0(t) - \left[\sum_{k=1}^{K} \tilde{a}_k(t)\phi_k(x_j) + \tilde{a}_k^*(t)\phi_k^*(t) \right] \right|^2. \tag{4}$$

The solution of problem (4) can be explicitly (and compactly) written as

$$\hat{\boldsymbol{a}}(t) := \left(\boldsymbol{\Phi}^H \boldsymbol{\Phi}\right)^{-1} \boldsymbol{\Phi}^H \boldsymbol{u}(t), \tag{5}$$

where $(\cdot)^H$ denotes the conjugate-transpose of a matrix or vector, $\boldsymbol{u}(t) = [u^*(t,x_0), \ldots, u^*(t,x_{J-1})]^H$ is the $J \times 1$ vector of observations at time t, $\boldsymbol{\Phi} = [\phi_K^* \cdots \phi_1^* \;\; \phi_0 \;\; \phi_1 \cdots \phi_K]$ is the $J \times (2K+1)$ matrix with columns given by

$$\phi_k := \begin{bmatrix} \phi_k(x_0) \\ \vdots \\ \phi_k(x_{J-1}) \end{bmatrix}, \quad \text{and} \quad \hat{\boldsymbol{a}}(t) = \begin{bmatrix} \hat{a}_K^*(t) \\ \vdots \\ \hat{a}_1^*(t) \\ \hat{a}_0(t) \\ \hat{a}_1(t) \\ \vdots \\ \hat{a}_K(t) \end{bmatrix} \tag{6}$$

is a $2K+1$ vector that contains the LS estimates of the Fourier coefficients of $u(t,x)$.

Remark 1 *The coefficients in $\hat{\boldsymbol{a}}(t)$ are* estimates *because we assume a truncation to order K when we specify problem* (4)*. The truncation implies that $\hat{a}_k(t) = 0$ for $|k| > K$, while the true coefficients $a_k(t)$ can be non-zero for any k.*

Given the empirical estimates in Eq. (5) we construct a (truncated) slave system with Fourier coefficients $b_k(t)$ that evolve over time according to the nonlinear set of ODEs

$$\dot{b}_k = b_k\left(\alpha\omega_0^2 k^2 + i\beta\omega_0^3 k^3 - \gamma\omega_0^4 k^4\right) - \frac{1}{2} ik\omega_0 \sum_{\ell=-K}^{K} b_\ell b_{k-\ell} + \sum_{j=0}^{K} D_{kj}(\hat{a}_j - b_j), \quad k = 0, \ldots, K, \tag{7}$$

subject to $b_k(t) = 0$ for $|k| > K$ and $b_k(t) = b_{-k}^*(t)$ for every k. The first two terms in (7) mimic the master model of Eq. (3), and $\left\{D_{kj} \in \mathbb{C} : \;\; k, j \in \{0, \ldots, K\}\right\}$ are the coefficients of a $(K+1) \times$

$(K+1)$ coupling matrix that we denote as $\boldsymbol{D}$. We assume identical parameters (α,β,γ) in the master and slave models for the moment.

The field of the slave system is constructed from the Fourier modes obtained via Eq. (7), namely,

$$v_K(x,t) := \sum_{k=-K}^{K} b_k(t)\phi_k(x)$$

for $t \in [0,T]$ and periodic boundary condition $v_K(t,x) = v_K(t,x+X)$. Since $b_k(t) = b^*_{-k}(t)$ for $k = -K,\ldots,-K$, it follows that the signal is real, i.e., $v_K(t,x) \in \mathbb{R}$.

Remark 2 *Truncation of the Fourier modes amounts to a spatial discretization. If we let* $v(x,t) := \lim_{K\to\infty} v_K(t,x)$ *be the limit field generated by the slave model, then the signal* $v(t,x)$ *may display small-scale spatial effects which are not present in the truncation approximation* $v_K(t,x)$ *if* K *is too small. If those small-scale effects are of interest, one needs to increase* K *in order to obtain a finer spatial resolution.*

C. Identical synchronization

Assume that the master system is integrated numerically using a truncation scheme similar to the slave model. To be specific, assume that $u(t,x) \approx u_M(t,x)$, where

$$u_M(t,x) := \sum_{k=-M}^{M} \bar{a}_k(t)\phi_k(x), \tag{8}$$

and the coefficients $\bar{a}_k(t)$ evolve over time according to the set of ODEs

$$\dot{\bar{a}}_k = \bar{a}_k\left(\alpha\omega_0^2k^2 + i\beta\omega_0^3k^3 - \gamma\omega_0^4k^4\right) - \frac{1}{2}ik\omega_0\sum_{\ell=-M}^{M}\bar{a}_\ell\bar{a}_{k-\ell},, \tag{9}$$

for $k = 0,\ldots,M$, subject to $\bar{a}_k(t) = 0$ for $|k| > M$ and $\bar{a}_k(t) = \bar{a}^*_{-k}(t)$ for all k, so as to guarantee that $u_M(t,x) \in \mathbb{R}$. We remark that the Fourier coefficients in (2) and (8) are different, in general, for finite K, hence the notation $\bar{a}_k(t)$ for the approximation versus $a_k(t)$ for the true master system.

We are interested in the synchronization error between the master and slave models, which we denote as

$$\mathscr{E}(t,x) := u_M(t,x) - v_K(t,x), \quad t \in [0,T], \quad x \in \mathbb{R}. \tag{10}$$

It is relatively simple to show that, when the truncation order is the same in the two models $(K = M)$ and we choose a suitable coupling matrix $\boldsymbol{D}$, $\mathscr{E}(t,x) \to 0$ for all x provided that the initial

conditions $u_M(0,x)$ and $v_K(0,x)$ are sufficiently close. This is the notion of *local synchronization* as defined, e.g., in [38]. The proposition below provides a precise statement and a formal proof of this result.

Proposition 1 *Assume that the observations of the master system are $u(t,x_j) = u_M(t,x_j)$, for $j = 0,\ldots,J-1$, and $J \geq 2M+1$. If*

(i) $|u|_\infty := \sup_{x\in\mathbb{R};t\in[0,T]} |u_M(t,x)| < \infty$,

(ii) $K = M$ *and*

(iii) $\boldsymbol{D} = D\boldsymbol{I}$, *where $\boldsymbol{I}$ is the identity matrix and $D \in \mathbb{R}^+$,*

then the synchronization error field has a stationary point at $\mathscr{E}(t,x) = 0$ whenever D is sufficiently large.

Proof: Since $K = M$, the observations have the form $u_K(t,x_j)$, $j = 0,\ldots,J-1$. The assumption $J \geq 2M+1$ ensures that Eq. (5) yields the coefficients $\bar{a}_k$ exactly, i.e., $\hat{a}_k = \bar{a}_k$ for $k = 0,\ldots,K$, with $\bar{a}_k = 0$ when $|k| > K$ and $\bar{a}_k = \bar{a}^*_{-k}$ for all k.

Let us denote $\boldsymbol{b}(t) := \left[b_0^*(t),\ldots,b_K^*(t)\right]^H$ and $\bar{\boldsymbol{a}}(t) := \left[\bar{a}_0^*(t),\ldots,\bar{a}_K^*(t)\right]^H$. Then, the systems of ODEs (9) and (7) yield, respectively,

$$\dot{\bar{\boldsymbol{a}}} = \boldsymbol{\Psi}(\boldsymbol{\theta},\omega_0)\bar{\boldsymbol{a}} - \frac{1}{2}i\omega_0\boldsymbol{\eta}(\bar{\boldsymbol{a}}), \tag{11}$$

$$\dot{\boldsymbol{b}} = \boldsymbol{\Psi}(\boldsymbol{\theta},\omega_0)\boldsymbol{b} - \frac{1}{2}i\omega_0\boldsymbol{\eta}(\boldsymbol{b}) + \boldsymbol{D}\,(\bar{\boldsymbol{a}} - \boldsymbol{b}), \tag{12}$$

were $\boldsymbol{\theta} = [\alpha,\beta,\gamma]^\top$ is the 3×1 parameter vector, $\boldsymbol{\Psi}(\boldsymbol{\theta},\omega_0)$ is a $(K+1)\times(K+1)$ diagonal matrix with k-th diagonal entry $[\boldsymbol{\Psi}]_{kk} = \alpha\omega_0^2k^2 + i\beta\omega_0^3k^3 - \gamma\omega_0^4k^4$ and $\boldsymbol{\eta}(\boldsymbol{c})$ is a $(K+1)\times 1$ vector for which the k-th entry is $[\boldsymbol{\eta}(\boldsymbol{c})]_k = k\sum_{\ell=-K}^{K} c_\ell c_{k-\ell}$.

If we define

$$e_k(t) := \bar{a}_k(t) - b_k(t) \quad \text{and} \quad \boldsymbol{e}(t) := [e_0^*(t),\ldots,e_K^*(t)]^H,$$

and then subtract (12) from (11), we obtain the system of ODEs

$$\dot{\boldsymbol{e}} = \boldsymbol{\chi}(\boldsymbol{e}), \tag{13}$$

where $\boldsymbol{\chi}(\boldsymbol{e}) := (\boldsymbol{\Psi}(\boldsymbol{\theta},\omega_0) - \boldsymbol{D})\,\boldsymbol{e} - \frac{1}{2}i\omega_0\,(\boldsymbol{\eta}(\bar{\boldsymbol{a}}) - \boldsymbol{\eta}(\bar{\boldsymbol{a}} - \boldsymbol{e}))$. It is apparent from Eq. (10) that the synchronization error admits a Fourier series representation with coefficients $e_k(t)$,

$$\mathscr{E}(t,x) = \sum_{k=-K}^{K} e_k(t)\phi_k(t), \tag{14}$$

hence the field $\mathscr{E}(t,x)$ has a stationary point at $\mathscr{E}(t,x)=0$ if, and only if, the ODE (13) has a stationary point at $\boldsymbol{e}(t)=\mathbf{0}$. In order to prove that $\boldsymbol{e}(t)=0$ is a stationary point it is sufficient to show that the Jacobian of $\boldsymbol{\chi}(\boldsymbol{e})$, denoted $\boldsymbol{J}_{\chi}(\boldsymbol{e})$, is negative definite at $\boldsymbol{e}=0$, i.e., $\boldsymbol{J}_{\chi}(\mathbf{0}) \prec \mathbf{0}$ [40].

Some straightforward calculations show that

$$\boldsymbol{J}_{\chi}(\boldsymbol{e}) = \boldsymbol{\Psi}(\boldsymbol{\theta},\omega_0) - i\omega_0 \boldsymbol{Q}(\bar{\boldsymbol{a}},\boldsymbol{e}) - \boldsymbol{D},$$

where the matrix $\boldsymbol{Q}(\bar{\boldsymbol{a}},\boldsymbol{e})$ is

$$\boldsymbol{Q}(\bar{\boldsymbol{a}},\boldsymbol{e}) = \begin{bmatrix} 0 & 0 & \cdots & 0 \\ \bar{a}_1 - e_1 & \bar{a}_0 - e_0 & \cdots & \bar{a}_{1-K} - e_{1-K} \\ \bar{a}_2 - e_2 & \bar{a}_1 - e_1 & \cdots & \bar{a}_{2-K} - e_{2-K} \\ \vdots & \vdots & \ddots & \vdots \\ \bar{a}_K - e_K & \bar{a}_{K-1} - e_{K-1} & \cdots & \bar{a}_0 - e_0 \end{bmatrix}.$$

Assumption (i) in the statement of Proposition 1 implies that $\sup_{k,t} |\bar{a}_k(t)| < \infty$ which, in turn, implies that there exists some real constant $D_o < \infty$ such that, for every $D > D_o$,

$$\boldsymbol{J}_{\chi}(0) = \boldsymbol{\Psi}(\boldsymbol{\theta},\omega_0) - i\omega_0 \boldsymbol{Q}(\bar{\boldsymbol{a}},\mathbf{0}) - D\boldsymbol{I} \prec 0.$$

□

Remark 3 *The coupling matrix $\boldsymbol{D}$ can be chosen to be non-diagonal and still obtain local synchronization. Simply note that Eq.* (13) *has a stationary point at $\boldsymbol{e}(t)=\mathbf{0}$ whenever $\boldsymbol{\Psi}(\boldsymbol{\theta},\omega_0) - i\omega_0\boldsymbol{Q}(\bar{\boldsymbol{a}},\mathbf{0}) - \boldsymbol{D}$ is negative definite.*

Remark 4 *We have introduced the coupling term $\boldsymbol{D}(\hat{\boldsymbol{a}}-\boldsymbol{b})$, that leads to synchronization, in the ODE of the Fourier coefficients* (12)*. The synchronization schemes in [30, 33, 34] are similar but the coupling is introduced as an additional term directly in Eq.* (1)*.*

The study of synchronization schemes for chaotic models based on a diffusive term (often called 'nudging' in the context of data assimilation [28, 30]) can be traced back to the 90s, with the seminal paper by Pecora and Carroll [41].

D. Numerical results

Proposition 1 guarantees that the slave system attains identical synchronization with the master system only when their initial conditions are sufficiently close. Our computer experiments,

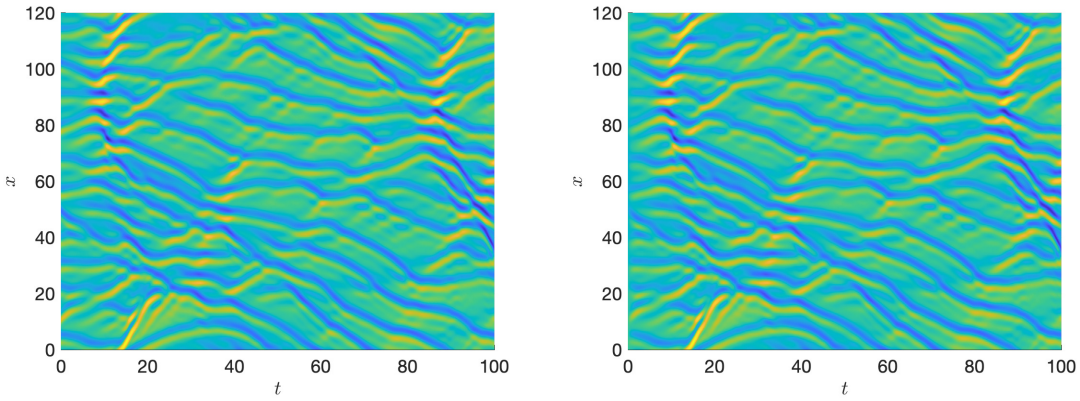

(a) $u_K(t,x)$ (b) $v_K(t,x)$

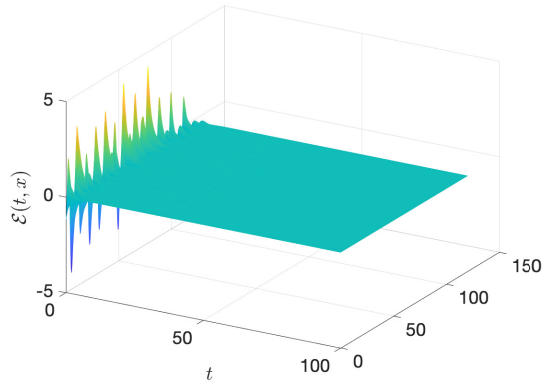

(c) $\mathscr{E}(t,x) = u_K(t,x) - v_K(t,x)$

Figure 1: **(a)** Real signal $u_K(t,x)$ generated by the master model, with $K = 32$ Fourier modes ($2K+1 = 65$ coefficients), $T = 100$ and $X = 120$. **(b)** Real signal $v_K(t,x)$ generated by the slave model with the same values of K, T and X, and a coupling constant $D = 1$. **(c)** Synchronization error. We see how the large error at time $t = 0$ due to the different initializations of the two systems vanishes quickly.

however, show that the scheme is robust and synchronization is achieved even when the initial conditions are significantly apart. These numerical results are discussed below.

Figure 1 shows the results of a computer simulation of the master and slave models with $M = K = 32$ Fourier modes, a time horizon of $T = 100$ time units, a spatial period $X = 120$ and parameter values $\alpha = 1.15$, $\beta = -0.05$ and $\gamma = 0.98$. Observations are collected at positions $x_j = j$ for $j = 0,\ldots,X-1$, hence $J = X = 120 > 2K+1 = 65$. Numerical integration has been carried out using an Euler scheme with (sufficiently small) time step $h = 0.005$, but higher order

methods can obviously be used as well –the setting described in this section does not preclude the use of any numerical scheme. The coupling matrix for this simulation is $\boldsymbol{D} = D\boldsymbol{I}$ with $D = 1$.

The Fourier coefficients of the slave model are initialized as $b_{-1}(0) = b_1(0) = 0.5$ and $b_k(0) = 0$ otherwise. In order to have a significantly different initialization in the master model, we run a simulation of the KS equation with coefficients $\tilde{a}_k(t)$ and the same initialization as in the slave model, i.e., $\tilde{a}_{-1}(0) = \tilde{a}_1(0) = 0.5$ and $\tilde{a}_k(0) = 0$ for $|k| \neq 1$. Then we record the coefficient values at time $T = 100$ and use them as an initial condition for the master system, i.e., $\bar{a}_k(0) = \tilde{a}_k(T)$. This procedure yields very different initial values of the master and slave Fourier coefficients and it also removes any transient regimes in the simulation of the master model.

Figure 1a shows the signal $u_K(t,x)$ generated by the master model for $t \in [0,100]$ and $x \in [0,120)$, while Figure 1b displays the field $v_K(t,x)$ that results from the integration of the slave model. We observe the space-time patterns typical of the KS equation and the quick synchronization of the slave system. Indeed, Figure 1c displays the synchronization error $\mathscr{E}(t,x) = u_K(t,x) - v_K(t,x)$ and we see that, even if the initial conditions of the master and slave models differ very significantly (observe the large errors at time $t = 0$), $\mathscr{E}(t,x)$ becomes negligible within a short time interval.

Figure 2 enables a more accurate assessment of the synchronization error and its convergence. In particular, Figure 2a shows the normalized mean square error (MSE)

$$\bar{\mathscr{E}}^2(t) := \frac{\int_0^X \mathscr{E}^2(t,x)\mathrm{d}x}{\int_0^X u_K^2(t,x)\mathrm{d}x}, \tag{15}$$

versus time t. We observe how the normalized MSE decreases exponentially fast (notice the logarithmic scale of the vertical axis) and $\bar{\mathscr{E}}^2(t) < 10^{-10}$ already before $t = 20$.

Figure 2b shows again the normalized MSE $\bar{\mathscr{E}}^2(t)$ versus time for different choices of the coupling coefficient D. In physical terms, the normalized error in (15) is the power of the error signal relative to the power of the master signal. We observe how the coupling strength affects the synchronization rate but not the steady-state (normalized) error, which is below 10^{-30} for $D = 1,5,10$ and still converging at time $t = 100$ for $D = 0.5$. We also see how the coupling constant $D = 0.1$ is too small to lead to synchronization.

Finally, we assess the normalized MSE and the synchronization rate when the observations are noisy. To be specific, we run a set of simulations where the observations fed to the slave model are of the form $u_K(t,x_j) + w_j(t)$, and the noise terms $w_j(t)$ are independent white Gaussian processes with mean 0 and power spectral density $S_w(i\omega) \approx 0.15$. We observe that, in the presence

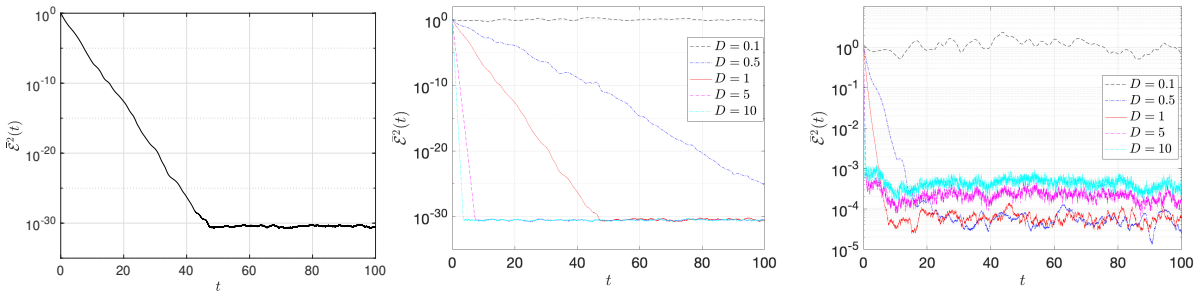

(a) (b) (c)

Figure 2: **(a)** Exponentially-fast convergence $\bar{\mathscr{E}}^2(t) \to 0$ of the normalized MSE. Noiseless data and $D = 1$. **(b)** Convergence of the normalized MSE $\bar{\mathscr{E}}^2(t) \to 0$ for different choices of the coupling constant $D > 0$ and noiseless data. **(c)** Convergence of the normalized MSE for different choices of $D > 0$ and noisy observations. Identical parameters $(\alpha, \beta, \gamma) = (1.15, -0.05, 0.98)$ in both the master and slave models.

of noise, the slave model still synchronizes more quickly as we increase the coupling coefficient D. However, the steady-state normalized MSE is higher for $D \in \{5, 10\}$ when compared to $D \in \{0.5, 1\}$. From this simulation, the best choice of coupling parameter is $D = 1$, which yields a steady-state error $\bar{\mathscr{E}}^2(t) \approx 10^{-4}$ already for $t > 7$.

III. PARAMETER ESTIMATION

Let us assume hereafter that the parameters $\boldsymbol{\theta} = [\alpha, \beta, \gamma]^\top$ of the master model are unknown and we wish to estimate them from the observations $\boldsymbol{u}(t) = [u^*(t, x_0), \ldots, u^*(t, x_{J-1})]^H$ described in Section II B and the corresponding Fourier coefficients $\hat{\boldsymbol{a}}(t)$ in Eq. (4), which are collected for $t \in [0, T]$.

The synchronization property of the KS slave model described in Section II can be used to estimate $\boldsymbol{\theta}$. To be specific, let $\hat{\boldsymbol{\theta}} = \left[\hat{\alpha}, \hat{\beta}, \hat{\gamma}\right]^\top$ be the parameters of the slave model. We have shown that, when $\hat{\boldsymbol{\theta}} = \boldsymbol{\theta}$, the slave system synchronizes and the error $\mathscr{E}(t, x)$ vanishes. However, the synchronization error can be written as the Fourier series in Eq. (14), where the coefficients $e_k(t) = \hat{a}_k(t) - b_k(t)$ depend on $\hat{\boldsymbol{\theta}}$ through $b_k(t)$. Following [26, 27], we argue that if the slave parameters $\hat{\boldsymbol{\theta}}$ are adapted over time in order to make $|e_k(t)| \to 0$, then the slave model attains identical synchronization, which can only be expected when $\hat{\boldsymbol{\theta}} \to \boldsymbol{\theta}$.

In Section III A we extend the slave model to account for the observation-driven adaptation of

the parameters $\hat{\boldsymbol{\theta}}(t)$ over time. Then, in Section III B, we present and discuss a set of numerical results that illustrate the validity of the method and its robustness when the observed data are noisy or the truncation order K is underestimated.

A. Slave model

We extend the slave model (12) by letting the parameters in $\boldsymbol{\theta}$ become dynamical variables. Specifically, the ODE governing the dynamics of the Fourier coefficients of the slave system is

$$\dot{\boldsymbol{b}} = \boldsymbol{\Psi}(\hat{\boldsymbol{\theta}}, \omega_0)\boldsymbol{b} - \frac{1}{2} i\omega_0 \boldsymbol{\eta}(\boldsymbol{b}) + \boldsymbol{D}\,(\hat{\boldsymbol{a}}_\top - \boldsymbol{b})\,, \tag{16}$$

where

$$\hat{\boldsymbol{\theta}}(t) = \begin{bmatrix} \hat{\alpha}(t) \\ \hat{\beta}(t) \\ \hat{\gamma}(t) \end{bmatrix} \quad \text{and} \quad \hat{\boldsymbol{a}}_\top(t) = \begin{bmatrix} \hat{a}_0(t) \\ \vdots \\ \hat{a}_K(t) \end{bmatrix}$$

is a truncated version of $\hat{\boldsymbol{a}}(t)$ in Eq. (6) that contains the last $K+1$ entries of the original vector. Recall that $\hat{a}_k(t) = \bar{a}_k(t)$ only when we assume the master model is truncated to $M = K$ modes, otherwise (if there is no truncation or $M \neq K$) $\hat{a}_k(t) \neq \bar{a}_k(t)$ in general.

We let the time evolution of the parameters $\hat{\boldsymbol{\theta}}(t)$ be driven by the mean power of the synchronization error $\mathscr{E}(t,x)$, denoted $\mathscr{E}^2(t) = \frac{1}{X}\int_0^X \mathscr{E}^2(t,x)\mathrm{d}x$. Since $\mathscr{E}(t,x)$ has the Fourier series representation in Eq. (14), Parseval's relation yields

$$\mathscr{E}^2(t) = \sum_{k=-K}^{K} |e_k(t)|^2 = \sum_{k=-K}^{K} |\hat{a}_k(t) - b_k(t)|^2$$

which, since $\hat{a}_k(t) = \hat{a}^*_{-k}(t)$ and $b_k(t) = b^*_{-k}(t)$, can be rewritten as

$$\mathscr{E}^2(t) = |\hat{a}_0(t) - b_0(t)|^2 + 2\sum_{k=1}^{K} |\hat{a}_k(t) - b_k(t)|^2.$$

The complexity of the slave model can be reduced if we adopt a slightly different synchronization error function, namely,

$$\mathscr{C}(t) := \sum_{k=0}^{K} |e_k(t)|^2 = \|\boldsymbol{e}(t)\|^2 = \|\hat{\boldsymbol{a}}_\top(t) - \boldsymbol{b}(t)\|^2, \tag{17}$$

where $\boldsymbol{e}(t) = \hat{\boldsymbol{a}}_\top(t) - \boldsymbol{b}(t)$. The difference between $\mathscr{E}^2(t)$ and $\mathscr{C}(t)$ is a scale factor and the contribution of the 0-th Fourier mode, namely,

$$\mathscr{C}(t) = \frac{1}{2}\left(\mathscr{E}^2(t) + |\hat{a}_0(t) - b_0(t)|^2\right).$$

Most importantly, $\mathscr{C}(t) = \mathscr{E}^2(t) = 0$ if, and only if, $\hat{a}_k(t) = b_k(t)$ for all $k \in \{-K, \ldots, K\}$. Hence, we can adopt the cost function $\mathscr{C}(t)$ to quantify the synchronization error and complete the derivation of the slave model.

Let $\nabla_{\hat{\boldsymbol{\theta}}}\mathscr{C} = \left[\frac{\partial \mathscr{C}}{\partial \hat{\alpha}}, \frac{\partial \mathscr{C}}{\partial \hat{\beta}}, \frac{\partial \mathscr{C}}{\partial \hat{\gamma}}\right]^\top$ denote the gradient of the synchronization error function with respect to the parameter vector $\hat{\boldsymbol{\theta}}$. In order to progressively reduce the power of the synchronization error, we let the slave parameters evolve in the direction opposite to the gradient of $\mathscr{C}$, namely,

$$\dot{\hat{\boldsymbol{\theta}}} = -\nabla_{\hat{\boldsymbol{\theta}}}\mathscr{C}. \tag{18}$$

Unfortunately, there is no closed-form expression for $\nabla_{\hat{\boldsymbol{\theta}}}\mathscr{C}$ and, hence, it is not possible to directly use Eq. (18). In order to construct a practical slave system, we first approximate the error function $\mathscr{C}(t)$ in terms of the parameters $\hat{\boldsymbol{\theta}}(t)$. This can be done if we linearize $\boldsymbol{b}(t)$ using a Taylor expansion around $\boldsymbol{b}(t-h)$, where $h > 0$ is some small time step. From Eq. (12), it is straightforward to see that the linearization yields

$$\begin{aligned}
\boldsymbol{b}(t) &= \boldsymbol{b}(t-h) + h\dot{\boldsymbol{b}}(t-h) + \mathscr{O}(h^2) \\
&\approx \boldsymbol{b}(t-h) + h\left(\boldsymbol{M}_h^H\hat{\boldsymbol{\theta}} - \frac{1}{2}i\omega_0\boldsymbol{\eta}\left(\boldsymbol{b}(t-h)\right) + \boldsymbol{D}\left(\hat{\boldsymbol{a}}(t-h) - \boldsymbol{b}(t-h)\right)\right),
\end{aligned} \tag{19}$$

where $\boldsymbol{M}_h = [\boldsymbol{m}_0 \cdots \boldsymbol{m}_K]$ is a $3 \times (K+1)$ complex matrix whose k-th column is

$$\boldsymbol{m}_k = b_k^*(t-h)\begin{bmatrix} \omega_0^2 k^2 \\ -i\omega_0^3 k^3 \\ -\omega_0^4 k^4 \end{bmatrix}, \tag{20}$$

hence, comparing with Eq. (12), $\boldsymbol{M}_h^H\hat{\boldsymbol{\theta}} = \boldsymbol{\Psi}(\hat{\boldsymbol{\theta}}, \omega_0)\boldsymbol{b}(t-h)$.

Substituting the approximation (19) in (17) yields, after some lengthy but straightforward calculations, an approximate gradient of the form

$$\begin{aligned}
\nabla_{\hat{\boldsymbol{\theta}}}\mathscr{C}(t) &\approx -h\boldsymbol{M}_h\left[\hat{\boldsymbol{a}}_\top(t) - \boldsymbol{b}(t-h) - h\dot{\boldsymbol{b}}(t-h)\right] \\
&= -h\boldsymbol{M}_h\left[\hat{\boldsymbol{a}}_\top(t) - \boldsymbol{b}(t-h) - h\left(\boldsymbol{M}_h^H\hat{\boldsymbol{\theta}} - \frac{1}{2}i\omega_0\boldsymbol{\eta}\left(\boldsymbol{b}(t-h)\right)\right.\right. \\
&\qquad \left.\left. + h\boldsymbol{D}\left(\hat{\boldsymbol{a}}_\top(t-h) - \boldsymbol{b}(t-h)\right)\right)\right].
\end{aligned} \tag{21}$$

Finally, we combine approximation (21), for the gradient of the error, and (12), for the Fourier coefficients $\boldsymbol{b}(t)$, to construct the slave model

$$\dot{\hat{\boldsymbol{\theta}}} = -\mu h\boldsymbol{M}_h\left[\hat{\boldsymbol{a}}_\top - \boldsymbol{b}_h - h\dot{\boldsymbol{b}}_h\right], \tag{22}$$

$$\dot{\boldsymbol{b}} = \boldsymbol{\Psi}(\hat{\boldsymbol{\theta}}, \omega_0)\boldsymbol{b} - \frac{1}{2}i\omega_0\boldsymbol{\eta}(\boldsymbol{b}) + \boldsymbol{D}\left(\hat{\boldsymbol{a}}_\top - \boldsymbol{b}\right), \tag{23}$$

where $\boldsymbol{b}_h = \boldsymbol{b}(t-h)$, $\dot{\boldsymbol{b}}_h = \dot{\boldsymbol{b}}(t-h)$, $\mu > 0$ is an adaptation rate parameter that can be chosen to speed up or slow down the dynamics of $\hat{\boldsymbol{\theta}}(t)$. Tuning μ and $\boldsymbol{D}$ allows for a trade-off between the time needed by the slave system to synchronize and the accuracy it achieves.

B. Numerical results

In this section we study, numerically, the ability of the slave model (22)-(23) to attain synchronization with the master system (2), and yield accurate estimates $\hat{\boldsymbol{\theta}}(t)$, when the master parameters $\boldsymbol{\theta} = [\alpha, \beta, \gamma]^\top$ are unknown.

1. *Simulation setup*

The simulation setup is similar to the computer experiments in Section II D. Figure 3 shows the results of a simulation run with $M = 64$ Fourier modes in the master system and $K = 64$ modes in the slave model (note that K modes implies $2K+1$ coefficients, $b_{-K}(t), \ldots, b_K(t)$, however $b_k(t) = b^*_{-k}(t)$). The length of the time interval is $T = 100$, the spatial period is $X = 120$ and the parameter values in the master system are $\alpha = 1.15$, $\beta = -0.05$ and $\gamma = 0.98$, which yield chaotic dynamics. Observations are collected at positions $x_j = \frac{j}{2}$ for $j = 0, 1, \ldots, 2X-1$, hence $J = 2X = 240 > 2K+1 = 129$. The ODEs (2) and (22)-(23) are numerically integrated using an Euler scheme with (a sufficiently small) time step $h = 0.005$ (but higher-order schemes can be used as well). The Fourier coefficients of the master and slave models are initialized in the same way as in Section II D, which yields a large error at time $t = 0$ (see Figure 3c). The initial parameter values at the slave system are $\hat{\boldsymbol{\theta}}(0) = [0, 0, 0]^\top$. The coupling matrix in (23) is $\boldsymbol{D} = D\boldsymbol{I}$ with $D = 1$ and the adaptation rate is $\mu = 200$.

2. *Synchronization and parameter estimation*

Figure 3a displays the field $u_K(t,x)$, $t \in [0,T]$, $x \in [0,X]$, generated by the master model, while Figure 3b displays the signal $v_K(t,x)$ generated by the slave model. Figure 3c shows that the synchronization error $\mathscr{E}(t,x) = u_K(t,x) - v_K(t,x)$ vanishes quickly despite the significantly different initializations of the two models.

For the same simulation run as in Figure 3, Figure 4a shows that the normalized MSE, $\bar{\mathscr{E}}^2(t)$

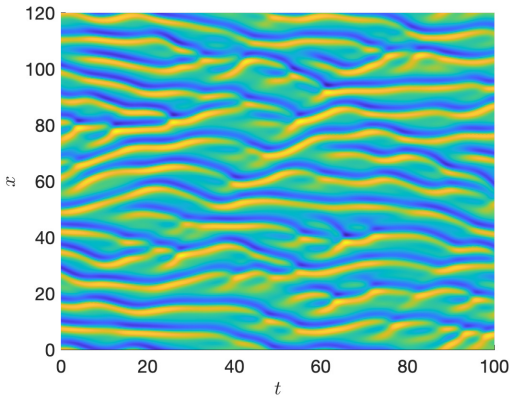

(a) $u_M(t,x)$

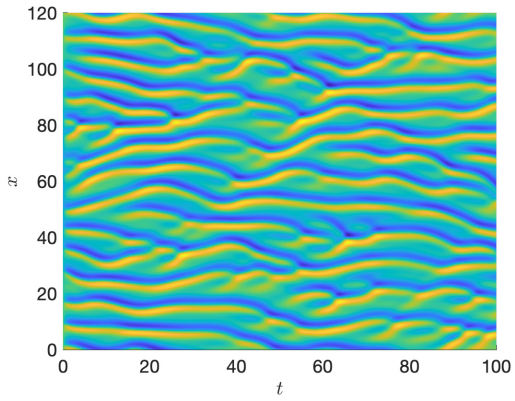

(b) $v_K(t,x)$

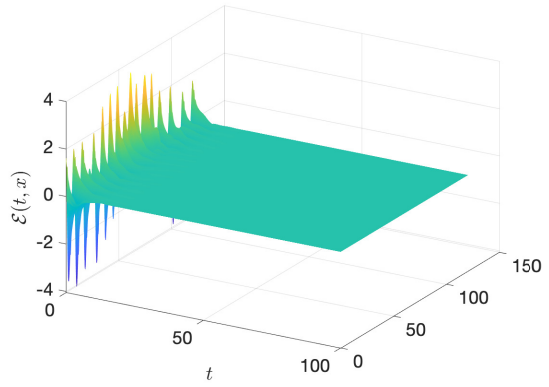

(c) $\mathscr{E}(t,x) = u_K(t,x) - v_K(t,x)$

Figure 3: **(a)** Real signal $u_K(t,x)$ generated by the master model, with $M = K = 64$ ($2K+1 = 129$ Fourier coefficients), $T = 100$ and $X = 120$. **(b)** Real signal $v_K(t,x)$ generated by the slave model with the same values of K, T and X, coupling constant $D = 1$, initial parameter values $\hat{\boldsymbol{\theta}}(0) = [0,0,0]^\top$ and parameter adaptation rate $\mu = 200$. **(c)** Synchronization error. We see how the large error at time $t = 0$ due to the different initializations of the two systems vanishes quickly.

as given in Eq. (15), decreases exponentially fast with time t. Recall that $\bar{\mathscr{E}}^2(t)$ is the normalized synchronization error between the master and slave systems. Figure 4b displays the parameter estimation errors $|\alpha - \hat{\alpha}(t)|^2$, $|\beta - \hat{\beta}(t)|^2$ and $|\gamma - \hat{\gamma}(t)|^2$ and shows that $\hat{\boldsymbol{\theta}}(t) \to \boldsymbol{\theta}$ exponentially fast as well. Note that, while estimation is very accurate, the errors are still decreasing after $T = 100$ time units.

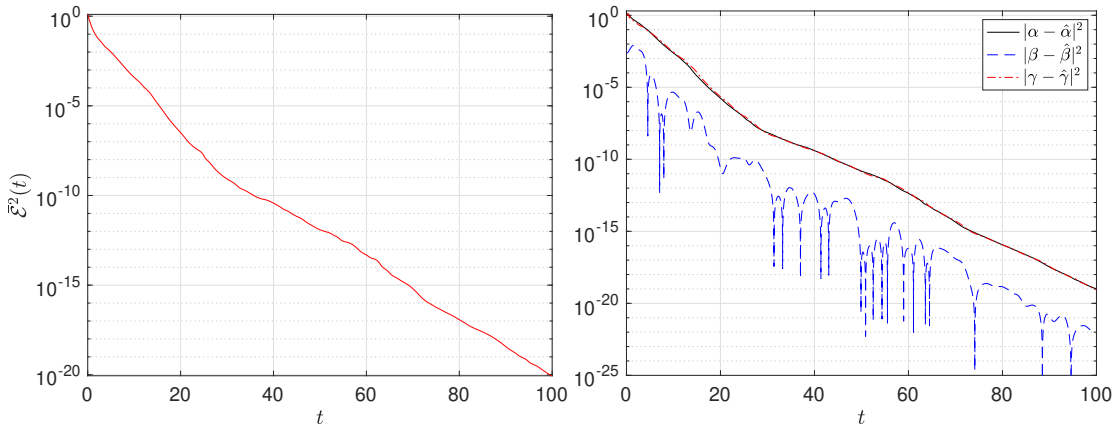

(a) Normalized error $\bar{\mathscr{E}}^2(t)$.

(b) Parameter estimation error

Figure 4: **(a)** Exponentially-fast convergence $\bar{\mathscr{E}}^2(t) \to 0$ of the normalized synchronization error with coupling constant $D = 1$ and adaptation rate $\mu = 200$. The initial parameter values in the slave model are $\hat{\boldsymbol{\theta}}(0) = [0,0,0]^\top$. The master parameters are $\boldsymbol{\theta} = [1.15, -0.05, 0.98]^\top$. **(b)** Squared estimation error for each of the unknown parameters in $\boldsymbol{\theta} = [\alpha, \beta, \gamma]^\top$.

3. *Coupling strength and adaptation rate*

The slave model can be 'tuned' by selecting different values of the coupling coefficient D and the adaptation rate μ. This is illustrated in Figure 5. Specifically, Figure 5a shows the normalized MSE, $\bar{\mathscr{E}}^2(t)$, for several values of the coupling coefficient D when the adaptation rate is kept fixed at $\mu = 200$. We see that a weak coupling ($D = 0.1$) does not guarantee synchronization or leads to slow convergence of the error ($D = 0.2$). Best results are obtained with $D = 0.5$ or $D = 1$, while further increasing the coupling strength results in slower convergence (unlike the results in Section II D with known parameters).

Next, we fix the value of the coupling coefficient to $D = 0.5$ in order to study the effect of varying the adaptation rate μ. Figure 5b shows the evolution of $\bar{\mathscr{E}}^2(t)$ for several values of μ. We observe that the smaller values ($\mu = 50,\ \ 100$) yield a slow decrease of the MSE. Increasing the adaptation rate to $\mu = 200$ significantly improves the convergence speed, but further increments ($\mu = 30,\ \ 400,\ \ 800$) do not result either in better accuracy or faster convergence.

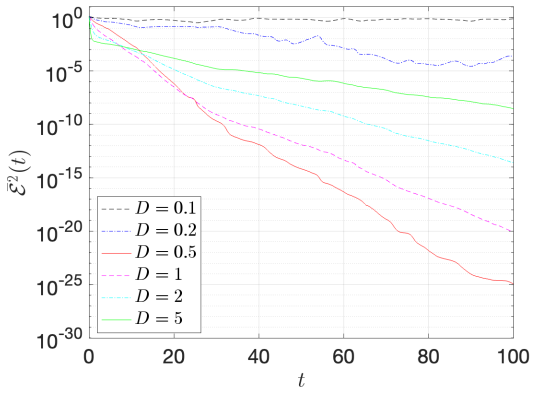

(a) Normalized error $\bar{\mathcal{E}}^2(t)$ with $\mu = 200$.

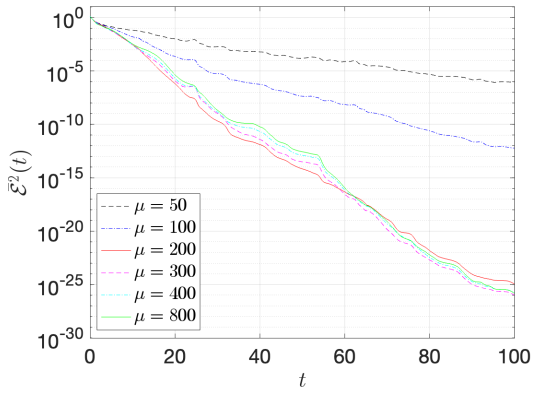

(b) Normalized error $\bar{\mathcal{E}}^2(t)$ with $D = 0.5$.

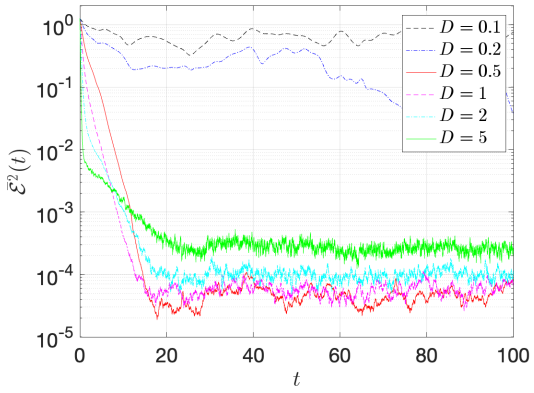

(c) $\bar{\mathcal{E}}^2(t)$ with $\mu = 200$ and noisy data.

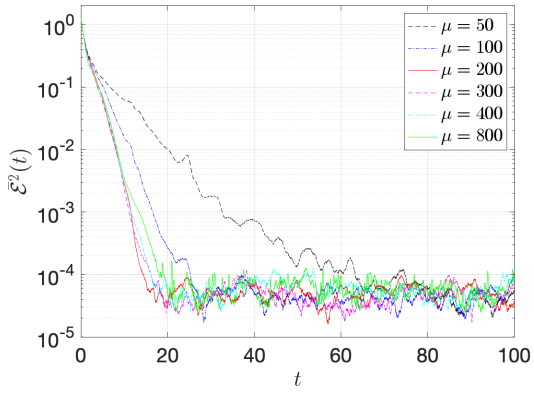

(d) $\bar{\mathcal{E}}^2(t)$ with $D = 0.5$ and noisy data.

Figure 5: **(a)** Normalized synchronization error $\bar{\mathcal{E}}^2(t)$ for different values of the coupling strength (D) with adaptation rate $\mu = 200$. The initial parameter values in the slave model are $\hat{\boldsymbol{\theta}}(0) = [0,0,0]^\top$. **(b)** $\bar{\mathcal{E}}^2(t)$ for different values of the adaptation rate (μ) with coupling strength $D = 0.5$. **(c)** $\bar{\mathcal{E}}^2(t)$ for different values of the coupling strength (D) with adaptation rate $\mu = 200$ and noisy data. **(d)** $\bar{\mathcal{E}}^2(t)$ for different values of the adaptation rate (μ) with coupling strength $D = 0.5$ and noisy data. The average SNR in the observations of plots (c) and (d) is 12 dB.

4. *Noisy observations*

For the remaining computer experiments we assume that the observed data from the master system are contaminated with Gaussian noise.

First, we have repeated the simulations of Figures 5a and 5b with noisy data. Specifically, we assume that the observations received at the slave model are of the form $u_K(t,x_j) + w_j(t)$, $j = 0,\ldots,J-1$, where the noise terms $w_j(t)$ are independent white Gaussian stochastic processes

with power spectral density $S_w(i\omega) \approx 0.17$, which corresponds to a signal-to-noise ratio (SNR) of 12 dB. Figure 5c displays the normalized synchronization error $\bar{\mathscr{E}}^2(t)$ for several values of the coupling strength D when the adaptation rate is kept fixed at $\mu = 200$. We see that small coupling ($D = 0.1, 0.2$) does not lead to synchronization; $D = 0.5, 1$ yield similar results, with fast convergence and an error floor (due to the observation noise) below 10^{-4}. Increasing the coupling strength further ($D = 2, 5$) still yields synchronization, but the error is higher. Figure 5d shows the normalized error $\bar{\mathscr{E}}^2(t)$ when $D = 0.5$ is fixed and the adaptation rate parameter μ takes values between 50 and 800. In this case, we observe that a small rate ($\mu = 50$) yields slow convergence of the error, although synchronization is attained after approximately 70 time units. For $\mu \geq 50$, the performance is similar for all values. Slightly faster convergence to the synchronized state is obtained for $\mu = 200, 300, 400$, but the error floor is very similar for $\mu = 100, 800$ as well.

5. *Number of Fourier modes*

Figure 6 shows the results of a set of computer experiments designed to study the effect of underestimating the number of coefficients K needed in the slave model. To this end, we generate the signal in the master system $u_M(t,x)$ using, again, $M = 64$ Fourier modes and then run slave models with order $K = 32, 34, \ldots, 66$. The coupling strength and the adaptation rate in all the slave models are $D = 0.5$ and $\mu = 200$, respectively. For all the simulations in this figure we have assumed that the observations are perturbed with white Gaussian noise with power spectral density $S_w(i\omega) \approx 0.17$ (average signal-to-noise ratio 12 dB). The results are averaged over 100 simulation runs, where the noise in the observations is generated independently for each run (while all other simulation parameters are kept the same).

Figure 6a shows the synchronization error versus the order K of the slave model. The error is an average over the interval $\left[\frac{4}{5}T, T\right]$ of the normalized MSE $\bar{\mathscr{E}}^2(t)$, i.e., $\bar{\mathscr{E}}^2 := \frac{5}{T}\int_{\frac{4T}{5}}^{T} \bar{\mathscr{E}}^2(t)\mathrm{d}t$. We observe how the synchronization error decreases consistently from $K = 32$ up to $K \approx 54$ and then stays approximately flat. This indicates that, even if the master model has Fourier modes up to order $M = 64$, $K \approx 54$ modes are sufficient to design a slave model that attains identical synchronization and yields accurate parameter estimates –this is coherent with early results on the existence and computation of inertial manifolds for the KS equation [42]. In particular, Figure 6b shows the evolution of the error $\bar{\mathscr{E}}^2(t)$ versus time for $K = 32, 38, 54, 64$. We observe that the synchronization error is nearly the same for $K = 54$ and $K = 64$, and two orders of magnitude

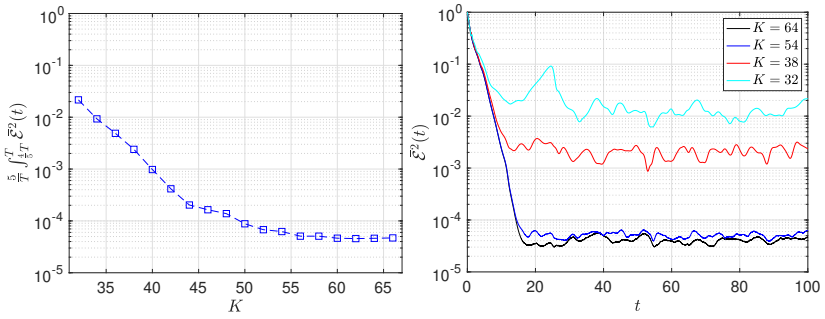

(a) Averaged normalized error for $M = 64$ and $K = 32, \ldots, 66$. Noisy data.

(b) $\bar{\mathscr{E}}^2(t)$ vs. time for $M = 64$ and $K = 32, 38, 54, 64$. Noisy data.

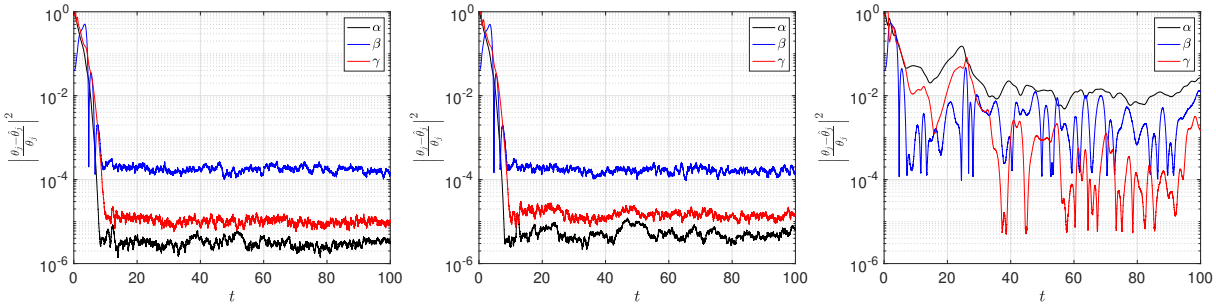

(c) Parameter estimation error with $M = 64$ and $K = 64$. Noisy data.

(d) Parameter estimation error with $M = 64$ and $K = 54$. Noisy data.

(e) Parameter estimation error with $M = 64$ and $K = 32$. Noisy data.

Figure 6: **(a)** Average over the interval $t \in \left[\frac{4T}{5}, T\right]$ of the normalized MSE, $\frac{5}{T}\int_{\frac{4}{5}T}^{T} \bar{\mathscr{E}}^2(t)\mathrm{d}t$, for $K = 32, \ldots, 64$ in the slave model. The master model is implemented with $M = 64$. The coupling strength is $D = 0.5$ and the adaptation rate is $\mu = 200$. The initial parameter values in the slave model are $\hat{\boldsymbol{\theta}}(0) = [0,0,0]^\top$ and the master parameters are $\boldsymbol{\theta} = [1.15, -0.05, 0.98]^\top$. The observations are contaminated with Gaussian noise (the average SNR is 12 dB). The error is almost equally small for all $K \geq 54$. **(b)** $\bar{\mathscr{E}}^2(t)$ for $K = 32, 38, 54, 64$ for the same set of simulations. **(c)** Normalized quadratic parameter estimation error for the three model parameters, $\boldsymbol{\theta} = [\alpha, \beta, \gamma]^\top$, when $K = 64$. **(d)** Normalized quadratic parameter estimation error when $K = 54$. **(e)** Normalized quadratic parameter estimation error when $K = 32$.

smaller than the error for $K = 32$. We point out, nevertheless, that $\bar{\mathscr{E}}^2(t)$ is normalized hence, even for $K = 32$, the power of the actual error is just $\approx 1\%$ of the power of the master signal $u_M(t,x)$.

Figures 6c, 6d and 6e show the normalized squared estimation error for the parameters in

$\boldsymbol{\theta} = [\alpha, \beta, \gamma]^\top$ when $K = 64$ (Fig. 6c), $K = 54$ (Fig. 6d) and $K = 32$ (Fig. 6e), respectively. Again, we see that the estimation error is almost the same with $K = 64$ and $K = 54$, while it is significantly higher for $K = 32$. Nevertheless, we again point out that these are normalized errors and, even for $K = 32$, they are around or below 1% for most of the simulation interval.

6. *Comparison with other methods*

Most methods for parameter estimation in the KS equation are offline [16–19, 21, 43]. They are designed for a different setup (possibly with scarce observations) and have a much higher computational cost than the online scheme introduced in Section III A. Comparisons should be carried out with other online methods.

The most similar scheme is the one by Pachev *et al.* [30]. The computational cost of both Pachev *et al.*'s method and the proposed scheme is dominated by the computation of the convolution $\tilde{b}_k = \sum_{\ell=-K}^{K} b_\ell b_{\ell-k}$ (see Eq. (7)), which has complexity $\mathcal{O}(K \log K)$. However, Pachev *et al.*'s method requires the computation of time derivatives of the master signal (i.e., either $\boldsymbol{u}_t(t)$ or $\hat{\boldsymbol{a}}_t(t)$), which are hard to compute in the presence of observational noise. Equations (22) and (23) involve $\hat{\boldsymbol{a}}$ alone (and *not* its derivative $\hat{\boldsymbol{a}}_t$) which makes the proposed method directly applicable (and robust, as shown in Sections III B 4 and III B 5) with noisy observations.

Within the class of statistical methods, a comparison can be carried out with the unscented Bucy-Kalman filter (UBKF) [44]. This is an online method that can be used to approximate the conditional mean and covariance matrix of the $(M+4) \times 1$ extended state vector $\boldsymbol{s}(t) = \begin{bmatrix} \boldsymbol{\theta} \\ \bar{\boldsymbol{a}}(t) \end{bmatrix}$ at any time t, given the observations $\boldsymbol{u}(\tau)$, $0 < \tau \leq t$. The UBKF relies on a quadrature or cubature scheme to approximate the nonlinearity of the KS equation. While other possibilities exist [45, 46], we have employed a spherical-radial cubature rule of degree 3 [45] which uses $L = 2(M+4)$ reference points. These L points are deterministically computed and they have to be propagated across the KS equation (in the same vein as one would do with a Monte Carlo method) for each step of the numerical integration scheme applied to the system of ODEs in (9).

The UBKF is one of the simplest statistical methods that can be applied to the parameter estimation problem for the KS equation, and yet its computational cost is much higher than the synchronization-based technique of Section III A or the method by Pachev *et al.* [30]. To be specific, both the UBKF and the proposed method have $\mathcal{O}(T)$ complexity (they are both online),

however the number of computations at each step of the Euler scheme is $\mathcal{O}(K \log K)$ for the proposed method versus $\mathcal{O}(K^2 \log K)$ for the UBKF (assuming $M = K$ Fourier modes in both cases). Also, the processing of the a $J \times 1$ observation vector $\boldsymbol{u}(t)$ takes $\mathcal{O}(J)$ operations for the proposed method, versus $\mathcal{O}(J^3)$ for the UBKF.

We have compared numerically the performance of the synchronization-based method given by Eqs. (22)-(23) with the UBKF algorithm within the same setup of Section III B 4. The UBKF is implemented as described above, with $M = 64$ and $L = 2(M+4) = 268$ reference points. We assume $K = M = 64$ in the slave model for the synchronization-based method.

Some results of the comparison are displayed in Figure 7. Specifically, Figure 7a shows the normalized synchronization error $\bar{\mathcal{E}}^2(t)$ attained by the proposed method and the UBKF. We observe that the UBKF converges more quickly, however the steady-state error of the proposed technique is one order of magnitude smaller. Both curves have been averaged over 20 independent simulation runs. With our code (running with Matlab R2023b on a MacBook Pro laptop with 64GB of memory and Apple M2 Max processor), the average run time of the synchronization-based method is ≈ 3 s for $T = 100$ and $h = 0.005$, versus ≈ 300 s for the UBKF in the same setup (this can be reduced by parallelization, though).

For the same set of simulations, Figures 7b, 7c and 7d show the normalized parameter estimation error for α, β and γ, respectively. Again, we see that convergence is faster for the UBKF but the synchronization-based method is more accurate, with errors at least two orders of magnitude smaller for all three parameters.

Remark 5 *We have compared the signal and parameter estimates directly in Figure 7. It should be noted that the UBKF also yields a covariance matrix for these estimates.*

7. *Dynamical regimes*

All the simulations presented so far correspond to the same set of parameter values $\boldsymbol{\theta} = [1.15, -0.05, 0.98]$, which yield a chaotic regime for Eq. (1). Figure 8 shows some illustrative results for different parameter sets, leading to different regimes of the KS equation.

As shown in [15], for fixed $\alpha = \gamma = 1$, the dynamics of the KS equation shift from chaotic to periodic as the parameter β is increased. Figures 8a, 8b and 8c display the space-time plot of

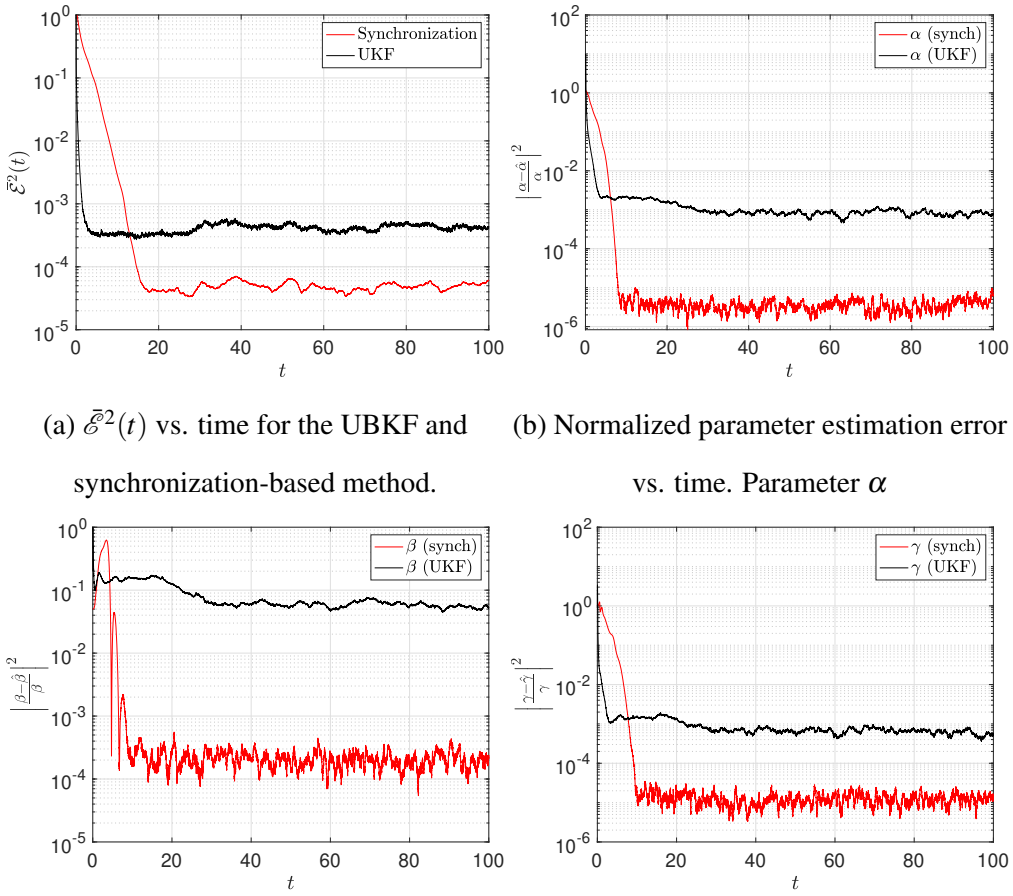

(a) $\bar{\mathscr{E}}^2(t)$ vs. time for the UBKF and synchronization-based method.

(b) Normalized parameter estimation error vs. time. Parameter α

(c) Normalized parameter estimation error vs. time. Parameter β

(d) Normalized parameter estimation error vs. time. Parameter γ

Figure 7: **(a)** Normalized MSE $\bar{\mathscr{E}}^2(t)$ versus time for the UBKF with $2(K+4)$ sigma-points and the proposed synchronization-based method with $M = K = 64$ Fourier modes. **(b, c, d)** Normalized parameter estimation errors versus. Observations are noisy, with average signal-to-noise ratio 12 dB. The coupling strength and adaptation rate are $D = 0.5$ and $\mu = 200$, respectively. The true parameters are $\boldsymbol{\theta} = [1.15, -0.05, 0.98]$, the initial values in the UBKF are $\hat{\boldsymbol{\theta}}(0) = [0.05, 0.05, 0.05]^\top$ and in the slave model are $\hat{\boldsymbol{\theta}}(0) = [0, 0, 0]^\top$. The results are averaged over 20 independent simulations.

the field $u(t,x)$ for $T = 100$ and $X = 120$ when $\beta = 0$, $\beta = 0.2$ and $\beta = 0.8$, respectively. We have run the synchronization-based method with $M = K = 64$ for each of these three scenarios and we present the average normalized synchronization error $\bar{\mathscr{E}}^2(t)$ (Figures 8d, 8e and 8f) and the evolution of the parameter estimates (Figures 8g, 8h and 8i). We observe that convergence and accuracy are similar in all three cases (just slightly faster for $\beta = 0.8$).

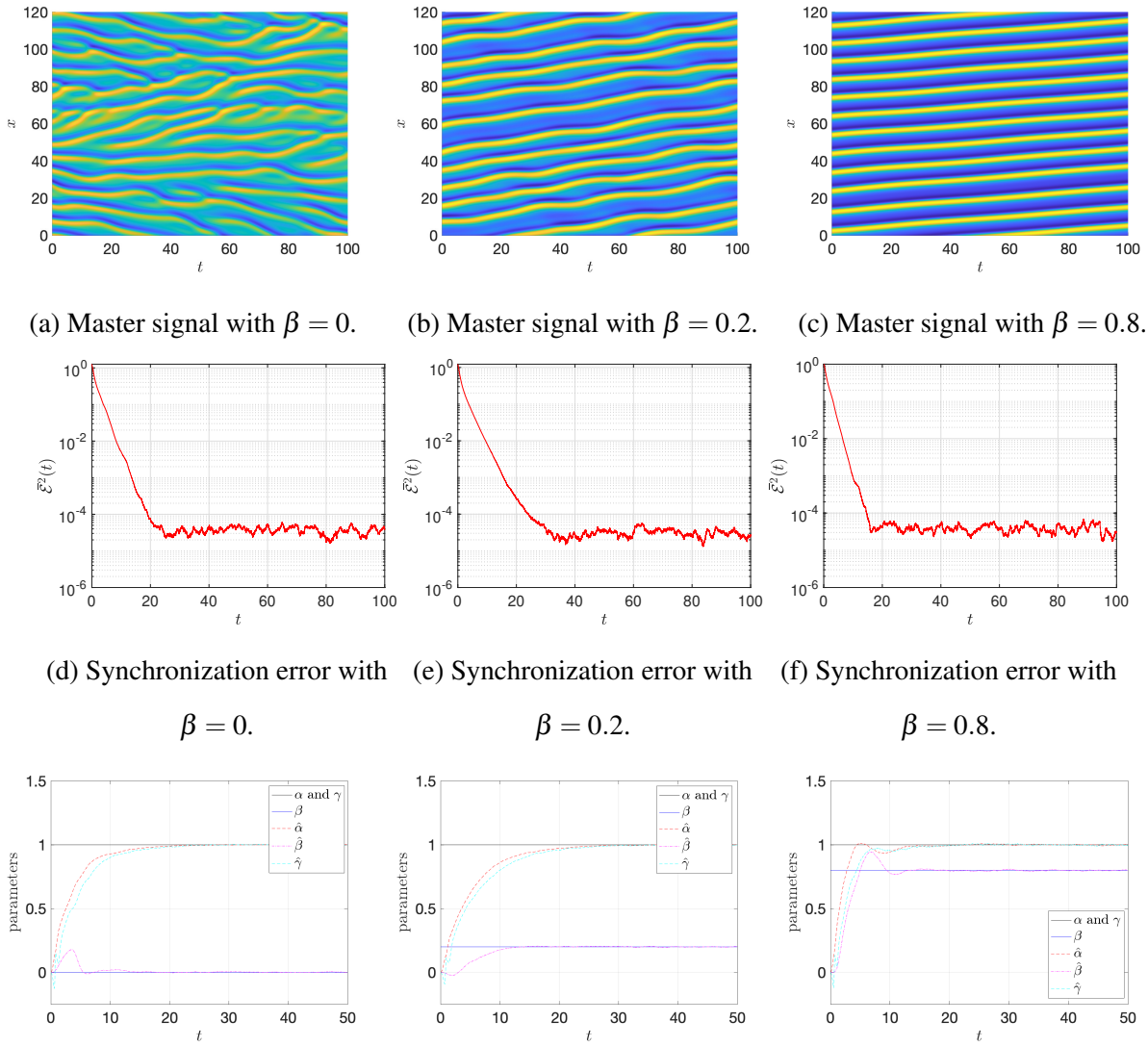

(a) Master signal with $\beta = 0$. (b) Master signal with $\beta = 0.2$. (c) Master signal with $\beta = 0.8$.

(d) Synchronization error with $\beta = 0$. (e) Synchronization error with $\beta = 0.2$. (f) Synchronization error with $\beta = 0.8$.

(g) Parameter errors with $\beta = 0$. (h) Parameter errors with $\beta = 0.2$. (i) Parameter errors with $\beta = 0.8$.

Figure 8: **(a, b, c)** Master signal with $\alpha = \gamma = 1$ and $\beta = 0$, $\beta = 0.2$ and $\beta = 0.8$, respectively. **(d, e, f)** Normalized synchronization MSE $\bar{\mathcal{E}}^2(t)$ versus time. **(g, h, i)** Parameter estimates versus time. The master and slave models are implmented with $M = K = 64$ Fourier modes. The coupling and adaptation rate parameters in the slave model are $D = 0.5$ and $\mu = 200$, respectively. Observations are noisy, with average SNR= 12 dB.

8. *Synchronization-based control*

Synchronization techniques can often be used for the implementation of control schemes [47] and the KS model has received specific attention from the control theory community [48, 49]. For

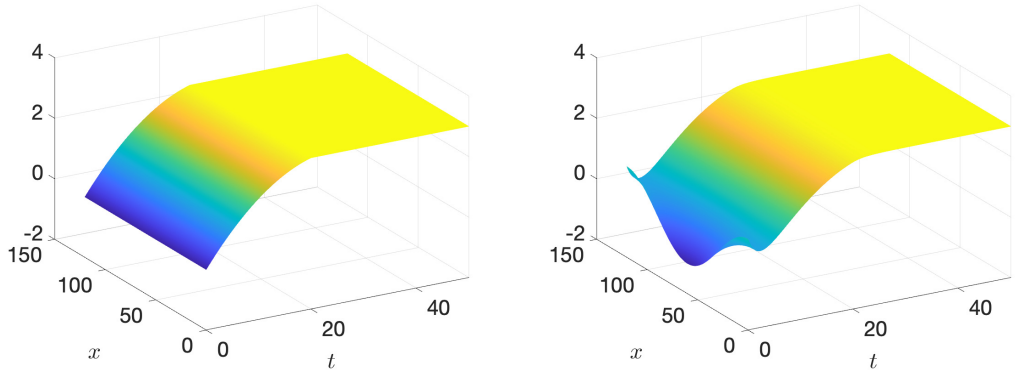

(a) Reference signal (observations).

(b) Slave model.

Figure 9: Control experiment. **(a)** Reference signal passed as observations to the slave model. **(b)** Slave model signal $u_K(x,t)$ with $K = 64$. The coupling strength and adaptation rate are $D = 0.5$ and $\mu = 200$, respectively. The initial parameter values are $\hat{\boldsymbol{\theta}}(0) = [0,0,0]^\top$.

the proposed method, one can think of the slave model (22)-(23) as a controlled system, where $u(t,x)$ is an input signal (i.e., not necessarily generated by a KS equation), $\boldsymbol{\theta} = [\alpha,\beta,\gamma]^\top$ is the control parameter and the aim is to make the slave signal $v_K(t,x)$ follow the reference input $u(t,x)$.

We have carried out a simple computer simulation to test whether the slave model (22)-(23) can be forced to follow an arbitrary input $u(x,t)$. This is just an illustrative experiment; a proper assessment of the proposed scheme in a control setup would require a detailed study.

The reference signal is depicted in Figure 9a. It is initialised at $u(0,x) = 0$ and then increases smoothly to reach $u(20,x) = 3$ for all $x \in [0,120)$; then $u(t,x) = 3$ for all $t \geq 20$. The parameter $\boldsymbol{\theta}$ is initialised as $\hat{\boldsymbol{\theta}} = [0,0,0]^\top$ like in the previous experiments. Also, the coupling coefficient is $D = 0.5$ and the adaptation rate is $\mu = 200$. We set $K = 64$ Fourier modes in the slave system.

Figure 9b shows the signal $v_K(t,x)$ of the slave model implemented with Eqs. (22)-(23). We observe how it reproduces the input signal accurately after a brief convergence period due to the mismatch in the initialization. Further study of the proposed scheme in more elaborate (and realistic) control problems is left for future work.

IV. CONCLUSIONS

We have investigated the synchronization properties and the estimation of the constant parameters of a generalized Kuramoto-Sivashinsky (KS) equation in 1-dimensional space. We have assumed the ability to collect observations over time from a *master* system with possibly unknown parameters and then we have tackled the design of a *slave* model driven by the observations. We have proved that, when the parameters of the slave model are fixed and identical to the master parameters, the slave system attains local identical synchronization. This is ensured by Proposition 1, which is a relatively simple result yet, to our best knowledge, not available in the previous literature on the KS equation. When the master parameters are unknown, the parameters of the slave system are time-varying and driven by a (suitably designed) ODE that depends on the observations and the Fourier coefficients of the slave model. We have conducted a detailed numerical study and shown that synchronization and accurate parameter estimation can be achieved, for different dynamical regimes (chaotic or periodic), even when the observations are noisy and the number of significant Fourier modes of the master system is underestimated.

The proposed scheme has turned out numerically robust to initialization errors (both in the signal and the parameters) in our simulations and it is designed to be implemented online and to estimate several parameters concurrently. Most statistical methods that have been aplied to the KS model [16–19] are offline (i.e., observations are processed iteratively in batches, rather than sequentially as they are collected) and they are computationally much more demanding. We have also compared the proposed scheme with the unscented Bucy-Kalman filter [44] (a popular *online* statistical estimation method for nonlinear systems) and found that the synchronization-based technique is more accurate and, even in this case, computationally lighter. However, the synchronization scheme requires continuous observation of the master system over a spatial grid (while most statistical schemes can work with discrete data sets) and does not provide a quantification of the expected error as Bayesian methods do. Compared to the scheme in [30], the proposed methodology can be robustly applied with noisy observations and is easier to implement. This is because it only demands the numerical integration of a relatively simple set of ODEs, while the method in [30] requires the construction of an orthonormal basis and the solution of a system of linear equations at each integration step.

Future work includes a stability analysis of the slave model with time-varying parameters, the combination of the proposed scheme with ensemble-based methods for data assimilation, the

extension of the methodology to other nonlinear PDEs or the design of control schemes. A simple, preliminary example of a controlled KS model forced to follow an *ad hoc* input signal has been presented in Section III B 8. Relevant nonlinear PDEs with a structure similar to Kuramoto-Sivashinsky's include, e.g., the Kawahara [6], Benney-Lin [50, 51] or Nikolaevsky [52] equations. These PDEs are similar enough to the KS model that the proposed methodology can be applied along the same lines described in this paper. Additional research will be needed to extend the stability analysis (possibly to a class of PDEs including these specific equations) and assess the numerical performance of the resulting schemes.

ACKNOWLEDGMENTS

This work has been partially supported by the Office of Naval Research (award N00014-22-1-2647) and Spain's *Agencia Estatal de Investigación* (ref. PID2021-125159NB-I00 TYCHE) funded by MCIN/AEI/10.13039/501100011033 and by "ERDF A way of making Europe".

DATA AVAILABILITY

The data that support the findings of this study are available within the article and its supplementary material.

---

[1] Y. Kuramoto and T. Tsuzuki. Persistent propagation of concentration waves in dissipative media far from thermal equilibrium. *Progress of Theoretical Physics*, 55(2):356–369, 1976.

[2] Y. Kuramoto. Diffusion-induced chaos in reaction systems. *Progress of Theoretical Physics Supplement*, 64:346–367, 1978.

[3] D. M. Michelson and G. I. Sivashinsky. Nonlinear analysis of hydrodynamic instability in laminar flames—II. numerical experiments. *Acta Astronautica*, 4(11-12):1207–1221, 1977.

[4] G. I. Sivashinsky. On flame propagation under conditions of stoichiometry. *SIAM Journal on Applied Mathematics*, 39(1):67–82, 1980.

[5] Z. Kadry. Bifurcation of traveling waves in a liquid film with broken time-reversal symmetry. *Physics Letters A*, 477:128895, 2023.

[6] J. Topper and T. Kawahara. Approximate equations for long nonlinear waves on a viscous fluid. *Journal of the Physical society of Japan*, 44(2):663–666, 1978.

[7] T. Tatsumi. Irregularity, regularity and singularity of turbulence. In *Turbulence and Chaotic Phenomena in Fluids*, pages 1–10, January 1984.

[8] R. Cuerno and A.-L. Barabási. Dynamic scaling of ion-sputtered surfaces. *Physical Review Letters*, 74(23):4746, 1995.

[9] N. A. Kudryashov. Exact solutions of the generalized Kuramoto-Sivashinsky equation. *Physics Letters A*, 147(5-6):287–291, 1990.

[10] R. W. Wittenberg and P. Holmes. Scale and space localization in the Kuramoto–Sivashinsky equation. *Chaos: An Interdisciplinary Journal of Nonlinear Science*, 9(2):452–465, 1999.

[11] C. Li and Z. Yang. Symmetry-breaking bifurcation in O(2)xO(2)-symmetric nonlinear large problems and its application to the Kuramoto–Sivashinsky equation in two spatial dimensions. *Chaos, Solitons & Fractals*, 22(2):451–468, 2004.

[12] C. D. Brummitt and J. C. Sprott. A search for the simplest chaotic partial differential equation. *Physics Letters A*, 373(31):2717–2721, 2009.

[13] Predrag Cvitanović, Ruslan L Davidchack, and Evangelos Siminos. On the state space geometry of the Kuramoto–Sivashinsky flow in a periodic domain. *SIAM Journal on Applied Dynamical Systems*, 9(1):1–33, 2010.

[14] N. B. Budanur and P. Cvitanović. Unstable manifolds of relative periodic orbits in the symmetry-reduced state space of the Kuramoto–Sivashinsky system. *Journal of Statistical Physics*, 167(3-4):636–655, 2017.

[15] N. A. Kudryashov and S. F. Lavrova. Dynamical features of the generalized Kuramoto-Sivashinsky equation. *Chaos, Solitons & Fractals*, 142:110502, 2021.

[16] C. Hurst, M. Zupanski, and X. Gao. The maximum likelihood ensemble smoother for the Kuramoto–Sivashinsky equation. *IMA Journal of Applied Mathematics*, 87(6):935–963, 2022.

[17] J. M. J. Huttunen, J. P. Kaipio, and H. Haario. Approximation error approach in spatiotemporally chaotic models with application to Kuramoto–Sivashinsky equation. *Computational Statistics & Data Analysis*, 123:13–31, 2018.

[18] F. Lu, K. K. Lin, and A. J. Chorin. Data-based stochastic model reduction for the Kuramoto–Sivashinsky equation. *Physica D: Nonlinear Phenomena*, 340:46–57, 2017.

[19] S. Martina-Perez, M. J. Simpson, and R. E. Baker. Bayesian uncertainty quantification for data-driven equation learning. *Proceedings of the Royal Society A*, 477(2254):20210426, 2021.

[20] K. M. Loew and R. M. Bradley. Parameter estimation for pattern formation induced by ion bombardment of solid surfaces using deep learning. *Journal of Physics: Condensed Matter*, 33(2):025901, 2020.

[21] S. H. Rudy, S. L. Brunton, and J. N. Kutz. Smoothing and parameter estimation by soft-adherence to governing equations. *Journal of Computational Physics*, 398:108860, 2019.

[22] G. Hu, Y. Lou, and P. D. Christofides. Model parameter estimation and feedback control of surface roughness in a sputtering process. *Chemical Engineering Science*, 63(7):1800–1816, 2008.

[23] U. Parlitz. Estimating model parameters from time series by autosynchronization. *Physical Review Letters*, 76:1232–1235, 1996.

[24] Anil Maybhate and RE Amritkar. Use of synchronization and adaptive control in parameter estimation from a time series. *Physical Review E*, 59(1):284, 1999.

[25] A. d'Anjou, C. Sarasola, F. J. Torrealdea, R. Orduna, and M. Grana. Parameter-adaptive identical synchronization disclosing Lorenz chaotic masking. *Physical Review E*, 63(4):046213, 2001.

[26] I. P. Mariño and J. Míguez. Adaptive approximation method for joint parameter estimation and identical synchronization of chaotic systems. *Physical Review E*, 72(5):057202, 2005.

[27] I. P. Mariño and J. Míguez. An approximate gradient-descent method for joint parameter estimation and synchronization of coupled chaotic systems. *Physics Letters A*, 351(4-5):262–267, 2006.

[28] H. D. I. Abarbanel, M. Kostuk, and W. Whartenby. Data assimilation with regularized nonlinear instabilities. *Quarterly Journal of the Royal Meteorological Society: A journal of the atmospheric sciences, applied meteorology and physical oceanography*, 136(648):769–783, 2010.

[29] H. D. I. Abarbanel, S. Shirman, D. Breen, N. Kadakia, D. Rey, E. Armstrong, and D. Margoliash. A unifying view of synchronization for data assimilation in complex nonlinear networks. *Chaos: An Interdisciplinary Journal of Nonlinear Science*, 27(12), 2017.

[30] B. Pachev, J. P. Whitehead, and S. A. McQuarrie. Concurrent multiparameter learning demonstrated on the Kuramoto–Sivashinsky equation. *SIAM Journal on Scientific Computing*, 44(5):A2974–A2990, 2022.

[31] Adrian Arellano-Delgado, Rosa Martha López-Gutiérrez, Miguel Ángel Murillo-Escobar, and Cornelio Posadas-Castillo. Master–slave outer synchronization in different inner–outer coupling network topologies. *Entropy*, 25(5):707, 2023.

[32] J Atencia-De la Ossa, C Orozco-Henao, and J Marín-Quintero. Master-slave strategy based in artificial intelligence for the fault section estimation in active distribution networks and microgrids. *International Journal of Electrical Power & Energy Systems*, 148:108923, 2023.

[33] Z. Tasev, L. Kocarev, L. Junge, and U. Parlitz. Synchronization of kuramoto–sivashinsky equations using spatially local coupling. *International Journal of Bifurcation and Chaos*, 10(04):869–873, 2000.

[34] L. Basnarkov, G. S. Duane, and L. Kocarev. Generalized synchronization and coherent structures in spatially extended systems. *Chaos, Solitons & Fractals*, 59:35–41, 2014.

[35] M. Jardak, I. M. Navon, and M. Zupanski. Comparison of sequential data assimilation methods for the Kuramoto–Sivashinsky equation. *International journal for numerical methods in fluids*, 62(4):374–402, 2010.

[36] H. Gotoda, M. Pradas, and S. Kalliadasis. Nonlinear forecasting of the generalized Kuramoto–Sivashinsky equation. *International Journal of Bifurcation and Chaos*, 25(05):1530015, 2015.

[37] S. G. Penny. Mathematical foundations of hybrid data assimilation from a synchronization perspective. *Chaos: An Interdisciplinary Journal of Nonlinear Science*, 27(12), 2017.

[38] M. M. Asheghan, J. Míguez, M. T. Hamidi-Beheshti, and M. S. Tavazoei. Robust outer synchronization between two complex networks with fractional order dynamics. *Chaos: An Interdisciplinary Journal of Nonlinear Science*, 21(3), 2011.

[39] Christo I Christov and KL Bekyarov. A Fourier-series method for solving soliton problems. *SIAM Journal on Scientific and Statistical Computing*, 11(4):631–647, 1990.

[40] P. Regalia. *Adaptive IIR Filtering in Signal Processing and Control*. Taylor and Francis, 1995.

[41] L. M. Pecora and T. L. Carroll. Synchronization in chaotic systems. *Physical review letters*, 64(8):821, 1990.

[42] C. Foias, M. S. Jolly, I. G. Kevrekidis, and E. S. Titi. On the computation of inertial manifolds. *Physics Letters A*, 131(7-8):433–436, 1988.

[43] X.L. Hu, T.B. Schon, and L. Ljung. A basic convergence result for particle filtering. *IEEE Transactions on Signal Processing*, 56(4):1337–1348, 2008.

[44] S. Sarkka. On unscented Kalman filtering for state estimation of continuous-time nonlinear systems. *IEEE Transactions on Automatic Control*, 52(9):1631–1641, 2007.

[45] Bin Jia, Ming Xin, and Yang Cheng. High-degree cubature kalman filter. *Automatica*, 49(2):510–518, 2013.

[46] Henrique MT Menegaz, João Y Ishihara, Geovany A Borges, and Alessandro N Vargas. A systematization of the unscented Kalman filter theory. *IEEE Transactions on Automatic Control*, 60(10):2583–2598, 2015.

[47] H. Zhang, D. Liu, and Z. Wang. *Controlling chaos: suppression, synchronization and chaotification*. Springer Science & Business Media, 2009.

[48] R. al Jamal and K. Morris. Distributed control of the Kuramoto-Sivashinsky equation using approximations. In *2015 American Control Conference (ACC)*, pages 3322–3327. IEEE, 2015.

[49] W. Kang and E. Fridman. Distributed sampled-data control of Kuramoto–Sivashinsky equation. *Automatica*, 95:514–524, 2018.

[50] D. J. Benney. Long waves on liquid films. *Journal of Mathematics and Physics*, 45(1-4):150–155, 1966.

[51] S. P. Lin. Finite amplitude side-band stability of a viscous film. *Journal of Fluid Mechanics*, 63(3):417–429, 1974.

[52] E. Simbawa, P. C. Matthews, and S. M. Cox. Nikolaevskiy equation with dispersion. *Physical Review E*, 81(3):036220, 2010.